Anal. Chem. **2002,** *74,* 1007−1016

A Low Dispersion Geometry for Microchip Separation Devices

Debashis Dutta and David T. Leighton, Jr.*

Department of Chemical Engineering, University of Notre Dame, Notre Dame, Indiana 46556

Curved channel geometries introduced on microchip separation devices to achieve greater separation distances often lead to large analyte dispersion, degrading the performance of these systems. While such electrokinetic dispersion may be minimized by reducing the channel width around the curved region, alternative strategies involving larger channel curvatures may be promising as well, depending on the application. For example, Culbertson et al. (*Anal. Chem.* 2000, *72,* 5814−5819) recently demonstrated the effectiveness of gentle spiral geometries in carrying out separations of small molecules. For moderate and large Peclet number systems, however, larger spiral geometries are necessary to diminish electrokinetic dispersion of solute slugs which may not conform to the needs of the microchip format. In this work, we investigate a modified spiral geometry with a wavy wall along the inner track of the channel. Analysis shows that such width profiling may significantly improve the performance of the spiral geometry, making the design effective for larger Peclet number or smaller radii systems. Numerical simulations performed to optimize these modified spirals suggest equating transit times along the inner and the outer track of the channel as a useful design criterion for minimizing electrokinetic dispersion. An analytical model has been formulated to derive the optimal channel parameters based on this criteria which compares well with the simulation results.

Significant progress has recently been made in demonstrating[2−4] the importance of microchip devices in carrying out analytical-scale separations. As theory suggests, a reduction in the length scale leads to a reduction in analysis time by as much as several orders of magnitude. Further, the portability of these devices and their potential to carry out parallel operations makes them an attractive alternative to conventional CE systems for laboratory-scale applications. The separation resolution, however, can be significantly limited due to the shorter dimensions of these miniaturized systems. To achieve higher resolutions, larger separation distances are often accommodated within a compact region using a serpentine layout involving channels with long straight sections followed by curved ends. While electrokinetic flows allow material transport with little dispersion due to nonuniform velocities in straight channel segments, they lead to large solute dispersion around turn geometries.[5,6] The dispersion in the curved section arises due to a differential in the transit time required to travel around the bend across different solute streamlines. Several studies[7−9] have shown that this differential in transit time can be well described in terms of differences in both path length and local solute velocity introduced by the curvature of the turn geometry. Such electrokinetic dispersion results in degradation in the performance of the serpentine geometry, reducing the benefit obtained from increased separation distances.

Theoretical and experimental studies carried out to understand the effect of turn geometries on the performance of microchip separation devices suggest several ways in which dispersion around curved channels may be minimized. The simplest and the most effective among these is a reduction in channel width around the curved region as explored by Paegel et al.[10] In their work, the class of designs that were investigated involved narrowed turn geometries connected to straight channel segments through symmetrically tapered sections. This strategy can be made even more effective by employing asymmetric narrowing sections that rotate the solute slug in a direction opposite to the direction of rotation in the turn, bending it into a crescent. This class of designs has been investigated recently,[9,11] and the optimized geometries have been demonstrated to outperform the symmetrically narrowed bends for a given minimum channel width. Alternatively, electrokinetic dispersion around curved channels may be reduced by increasing the radius of curvature of the turn geometry. An increase in the radius diminishes the shear flow in the channel, minimizing the spread of solute slugs in the presence of cross-channel diffusion. The weak dependence of such geometric dispersion on the channel curvature, however, requires very gentle turn geometries to achieve any significant reduction in electrokinetic dispersion. This in turn limits the separation distance that can be accommodated using a serpentine channel

* Corresponding author: (e-mail) dtl@nd.edu; (fax) 219-631-8366.

(1) Culbertson, C. T.; Jacobson, S. C.; Ramsey, J. M. *Anal. Chem.* **2000**, *72*, 5814−5819.
(2) Bruin, G. J. M. *Electrophoresis* **2000**, *21*, 3931−3951.
(3) Kutter, J. P. *Trends Anal. Chem.* **2000**, *19*, 352−363.
(4) Sanders, G. H. W.; Manz, A. *Trends Anal. Chem.* **2000**, *19*, 364−378.
(5) Jacobson, S. C.; Hergenröder, R.; Koutny, L. B.; Warmack, R. J.; Ramsey, J. M. *Anal. Chem.* **1994**, *66*, 1107−1113.
(6) Jacobson S. C.; Ramsey, J. M. *Electrophoresis* **1995**, *16*, 481−486.
(7) Culbertson, C. T.; Jacobson, S. C.; Ramsey, J. M. *Anal. Chem.* **1998**, *70*, 3781−3789.
(8) Griffiths, S. K.; Nilson, R. H. *Anal. Chem.* **2000**, *72*, 5473−5482.
(9) Molho, J. I.; Herr, A. E.; Mosier, B. P.; Santiago, J. G.; Kenny, T. W.; Brennen, R. A.; Gordon, G. B.; Mohammadi, B. *Anal. Chem.* **2001**, *73*, 1350−1360.
(10) Paegel, B. M.; Hutt, L. D.; Simpson, P. C.; Mathies, R. A. *Anal. Chem.* **2000**, *72*, 3030−3037.
(11) Griffiths, S. K.; Nilson, R. H. *Anal. Chem.* **2001**, *73*, 272−278.

10.1021/ac010718c CCC: $22.00
Published on Web 01/25/2002

layout for a given footprint area. A novel way of employing such gentle turn geometries into the microchip format is to replace the serpentine layout by spiral channels[1] with large radius of curvature. This class of designs is most effective for turn geometries with $R/W > O$ ($Pe = UW/D$), where R is the outer turn radius, W is the channel width, U is the solute velocity, and D is the molecular diffusivity of the solute molecules. The requirement of larger spirals render them less useful for systems with moderate and large Pe.

In this work, we investigate a simple width profiling strategy for the spiral channel layout to minimize geometric dispersion arising due to the channel curvature. The modified spirals involve a sinusoidal wavy inner wall that both increases the path length and decreases the average velocity along the inner track of the channel, minimizing variations in the transit time across different solute streamlines. Analytical and numerical techniques employed to derive optimum profiles suggest a significant improvement in the performance of these modified geometries over the unmodified spirals, particularly when $(W/R)Pe \gg 1$. For small Peclet number systems, the improvement diminishes since dispersion is completely dominated by molecular diffusion in the flow direction.

SCALING CONSIDERATIONS

To examine different separation channel geometries as well as to choose between them, it is essential to quantify the separation performance of these profiles in a way relevant to microfluidic channel design. To this end, consider the motion of two solute slugs through a microetched separation channel in an electrokinetically driven system. Because the solute velocity is proportional to the local electric field strength (E) in the channel,[12] the mean positions of the two analyte bands will separate a distance $\Delta L = \Delta\mu Et$ in separation time t. The proportionality constant $\Delta\mu$ here denotes the difference in the electrokinetic mobilities of the two analytes with an average mobility μ. Any such separation achieved on these miniaturized devices however, is often degraded due to dispersion experienced by the solute slugs as they travel along the microetched channel. This spread in the solute slugs may be quantified using the standard deviation of their concentration distributions σ_i, where the subscript stands for the ith analyte band. Note that the standard deviation of the two analyte bands will never be identical due to the fact that they are composed of different species. However, these species are often closely related and hence the two standard deviations may have a similar magnitude. In this situation, it may be more appropriate to work with an effective standard deviation σ defined to be the average or the maximum of the quantities σ_i.

The dispersion of analyte bands on a microchip separation device arises from both solute injection and flow and molecular diffusion. If these dispersion sources are assumed to act independently, the overall variance (σ^2) of the solute slug may be expressed as the sum of the variances contributed by each of the sources. A possible figure of merit quantifying the performance of any separation geometry is the separation resolution between the two analyte bands defined as

$$\mathrm{SR} = \frac{\Delta L}{\sigma} = \frac{\Delta\mu Et}{\sqrt{\sigma_{\mathrm{inj}}^2 + \sigma_{\mathrm{c}}^2}} \quad (1)$$

where σ_c^2 gives the variance introduced by the channel curvature in the presence of molecular diffusion. Since we are primarily interested in systems dominated by dispersion arising from curved channel geometries, we neglect the contribution from solute injection techniques[13] to the overall dispersion of the solute slugs. Further, we presume that the dispersion arising due to any curvature-induced shear flow in the channel may be described by the Taylor−Aris dispersion limit. This limit is achieved in separation channels of length $L > WPe$, which is satisfied for the spiral geometries considered here. In this situation, the overall dispersion of the analyte bands may be estimated as $\sigma_c = (2Kt)^{1/2}$, where K is the Taylor−Aris dispersivity, which depends on both the geometry and Peclet number. Upon substitution, the separation resolution may be rewritten as

$$\mathrm{SR} = \frac{\Delta\mu E}{\sqrt{2K}}\sqrt{t} = \Delta\mu\left(\frac{E}{2\mu K}\right)^{1/2}\sqrt{L} = \Delta\mu\left(\frac{EL}{2\mu D}\right)^{1/2}\sqrt{\frac{D}{K}} \quad (2)$$

As the choice for the electric field on microfluidic separation devices is often determined by dispersion due to Joule heating in the channel,[14] it has been suggested[9] that it is more appropriate to express the above scaling in terms of the electric field (E) and the separation length (L) rather than a maximum supply voltage. Based on the above considerations, eq 2 suggests that, for a given electric field strength and separation distance, the separation resolution is maximized for values of K/D close to unity (the minimum possible value). We examine the simple spiral geometry and other modified spiral profiles in light of this criterion.

DISPERSION: UNMODIFIED SPIRALS

As described earlier, analyte dispersion in an unmodified spiral geometry arises mainly due to a differential in the path length and solute velocity across different streamlines. Since this variation occurs over the width of the channel (W), an appropriate way of scaling dispersion around curved channels is to render all lengths dimensionless with respect to this channel width. To minimize electrokinetic dispersion, it is also desirable to use geometries that give rise to small shear flows in the channel. For a given channel width, this shear rate is inversely proportional to the channel curvature, and thus, in our analysis we focus on spiral designs with large normalized radii, i.e., $\alpha = W/R \ll 1$, where R is the outer radius of curvature for the curved geometry. Ultimately, the maximum radius of curvature allowable for these geometries is limited by the linear dimensions of the microchip device.

While the radius of curvature slowly changes in a spiral geometry, for $W/R \ll 1$, the influence of such changes on K/D in a single cycle is negligible. We shall thus consider only the case for constant W/R. The effect of such constant radius turn geometries on the performance of electrokinetic separation

(12) Cummings, E. B.; Griffiths, S. K.; Nilson, R. H.; Paul, P. H. *Anal. Chem.* **2000**, *72*, 2526−2532.

(13) Ermakov, S. V.; Jacobson, S. C.; Ramsey, J. M. *Anal. Chem.* **2000**, *72*, 3512−3517.

(14) Grushka, E.; McCormick, R. M.; Kirkland, J. J. *Anal. Chem.* **1989**, *61*, 241−246.

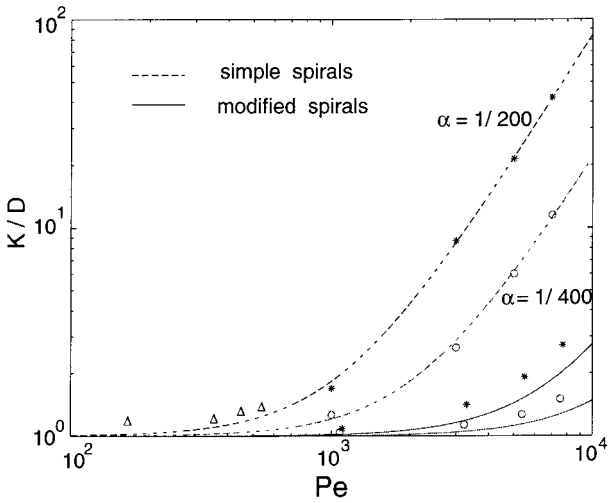

Figure 1. Taylor−Aris dispersion in curved channel geometries with constant turn radius. The dotted lines represent the functional dependence of *K*/*D* on *Pe* given by eq 4 whereas the symbols (○, ∗) were obtained using Monte Carlo simulations. The open symbol Δ denotes experimental data obtained from Culbertson et al.[1] for simple spiral geometries with normalized radius $1/\alpha = 437.5$.

systems has been throughly investigated by Griffiths and Nilson.[8] Their work demonstrates that solute dispersion around circular geometries with large turn radii may be modeled as that being caused by a straight channel section of identical length and having a simple linear velocity profile given by

$$v(y^*) = \mu E(1 + 2\alpha y^*); \quad 0 \le y^* \le 1 \tag{3}$$

Here $y^* = (R - r)/W$ describes the dimensionless coordinate in the transverse direction of the channel, with E being the electric field strength along its outer track. Proceeding further, the Taylor−Aris dispersivity describing the spread of the solute slugs in such systems may be shown[8] to be

$$\frac{K}{D} = 1 + \frac{(\alpha Pe)^2}{30}; \quad Pe = \frac{\mu E W}{D} \tag{4}$$

This dependence of the Taylor-Aris dispersivity on the Peclet number of the system has been depicted in Figure 1. From eq 4 it is clear that the simple spiral geometries are effective in minimizing solute dispersion for systems with $\alpha Pe < O(\sqrt{30})$. This may be achieved by employing either narrow separation channels or large turn curvature profiles. Culbertson et al.,[1] for example, demonstrated a large spiral geometry ($\alpha \approx 1/437$, $Pe \le 500$) for which the curvature-induced dispersion was negligible relative to other sources. In many cases, however, fabrication constraints or a requirement of a minimum solute throughput place a lower bound on the permissible channel width, while the size of the microchip itself limits the maximum allowable curvature for the profiles. In this work, we investigate a width profiling strategy that improves the separation performance of the spiral layout given some maximum turn curvature and a minimum channel width.

WIDTH PROFILING STRATEGIES

Given the constraint of a minimum channel width and a maximum turn curvature, a useful width profiling strategy that may minimize solute dispersion around curved geometries is the introduction of wavy walls along the inner track of the channel. These wavy walls both increase the path length and decrease the solute velocity along the inner track, thus minimizing variations in the transit time to travel around the separation channel. To see this, consider the motion of a solute slug through a curved channel geometry as shown in Figure 2. The side walls *AB* and *CD* of the channel both act as solute streamlines. In addition, there will be an infinite number of nonintersecting trajectories between *AB* and *CD*. Let the coordinate along any such streamline be given by *s*, and the local velocity (proportional to the electric field) be given by U_s. The transit time t is nothing more than the path integral of the inverse of the velocity over the entire channel:

$$t = \int_\Gamma \frac{1}{U_s}\,\mathrm{ds} \tag{5}$$

where Γ is the path. Because the total potential drop along any two paths is the same, we may define the spatial average velocity $\bar{U}_s$ in terms of the path length L. Note that this is the spatial average rather than the time average—if the velocity is not constant, these will not be the same. Adding and subtracting this value from the transit time yields

$$t = \frac{L}{\bar{U}_s} + \int_\Gamma \left(\frac{1}{U_s} - \frac{1}{\bar{U}_s}\right)\mathrm{ds}; \quad \bar{U}_s = \frac{\mu\Delta\phi}{L} \tag{6}$$

or, substituting in for the average velocity gives

$$t = \frac{L^2}{\mu\Delta\phi} + \frac{L^2}{\mu\Delta\phi}\left\langle \frac{\bar{U}_s}{U_s} - 1 \right\rangle \tag{7}$$

where < > denotes a spatial average along a path. From this expression, we see that the transit time is composed of two terms, one that is determined from the path length, and a second that is a result of variability in the velocity. The second term in eq 7 may be rearranged to yield

$$\frac{L^2}{\mu\Delta\phi}\left\langle \frac{\bar{U}_s}{U_s} - 1 \right\rangle = \frac{L^2}{\mu\Delta\phi}\left\langle \frac{(U_s - \bar{U}_s)^2}{\bar{U}_s U_s} \right\rangle \tag{8}$$

The above expression clearly shows that, for a given path and a potential drop, the effect of spatial variations in solute velocity is to always increase the transit time.

To eliminate dispersion, we wish to produce a wall profile such that all streamlines have the same transit time. To this end, we choose the outer wall of the channel to have a fixed radius R and the inner radius R_i to have the variable value

$$R_i = R - W - \epsilon W[1 - \cos(2\pi(\theta/\theta_0))] \tag{9}$$

Thus, the variability in width of the channel is characterized by the wavelength of periods (θ_0) and the amplitude of the variability given by ϵW. This function is also chosen so that the width is always $\ge W$, the width of the unmodified spiral.

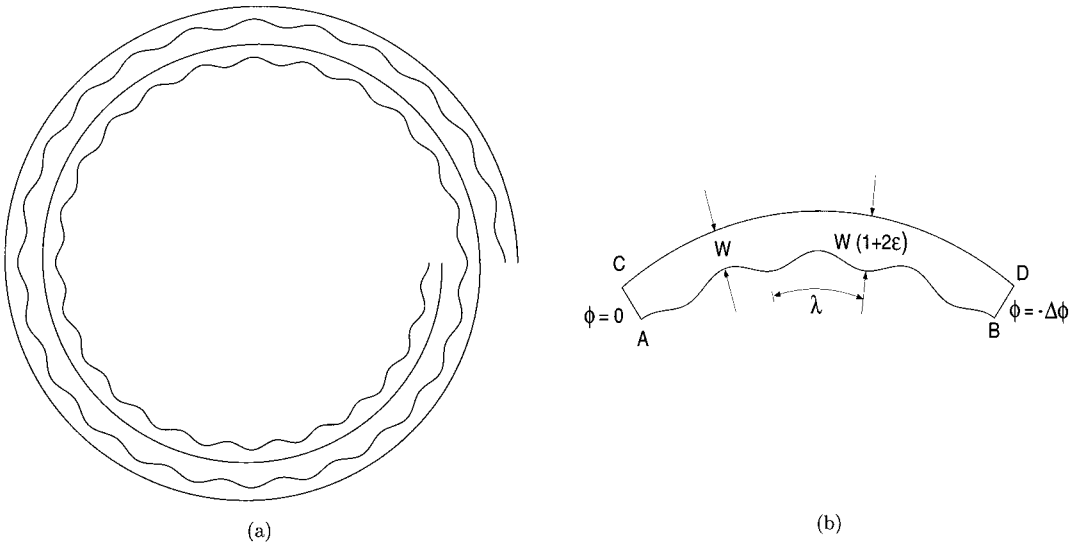

Figure 2. Spiral separation geometry with a wavy wall along the inner track of the channel.

To begin our analysis, we determine the effect of such profiling on the time for solute molecules to travel around the channel in the limit of large *Pe*. In this case, the effect may be calculated from the stream function[15] in the curved geometry. Although the exact solution to this problem requires numerical analysis, an asymptotic solution can be obtained in the limit when the channel curvature is large as compared to the wavelength of the periods along the inner wall and which in turn is much larger than the channel width; i.e., $R/W \gg \theta_0 R/W \gg 1$. In this situation, the effect of the channel curvature and width profiling on the overall dispersion of the solute slugs may be determined independently. Moreover, the dispersion due to the modified inner track would be quite similar to that produced by a wavy wall in a straight channel geometry as shown in Figure 3. The stream function in such a geometry may be obtained by solving the governing Laplace equation, which when rendered dimensionless with respect to the channel parameters of the wavy profile, yields

$$\frac{\partial^2 \psi}{\partial y^{*2}} + \delta^2 \frac{\partial^2 \psi}{\partial x^{*2}} = 0$$

with associated boundary conditions:

$$\psi = 0 \text{ at } y^* = 0;$$

$$\psi = 1 \text{ at } y^* = \frac{1}{f(x^*)} = 1 + \epsilon[1 - \cos(2\pi x^*)]$$

$$x^* = \frac{x}{\lambda}; \quad y^* = \frac{y}{W}; \quad \delta = \frac{W}{\lambda} \tag{10}$$

The above differential equation may be solved for small values of the parameter δ using a regular perturbation expansion[15,16] of the stream function given by $\psi = \psi_0 + \delta\psi_1 + \delta^2\psi_2 + \delta^3\psi_3 + \ldots$. Note that the convergence of the power series to ψ is strictly a consequence of the limit $\delta \rightarrow 0$ so that each successive term can be made arbitrarily small compared with the terms before it. In this situation, differential equations governing ψ_0, ψ_1, ψ_2, ... may be obtained upon substituting the power series in eq 10 and then individually equating the terms at each level in δ to zero. In a similar manner, the boundary conditions for ψ_0, ψ_1, ψ_2, ... may be derived upon substituting the power series for ψ into the boundary conditions governing the overall problem, i.e., eq 10. For small values of the parameter δ, the effect of the wavy boundary on ψ will be dominated by the leading order terms in the solution of this equation. The asymptotic solution presented here thus involves only the first three terms in the power series for ψ which, based on the regular perturbation technique, are governed by the following set of differential equations.

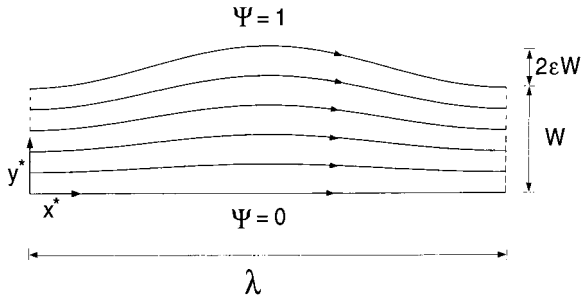

Figure 3. Solute streamlines in a straight channel geometry with a wavy wall.

$$\frac{\partial^2 \psi_0}{\partial y^{*2}} = 0 \qquad \psi_0 = 0 \text{ at } y^* = 0; \quad \psi_0 = 1 \text{ at } y^* = f(x^*)\ O(\delta^0)$$

$$\frac{\partial^2 \psi_1}{\partial y^{*2}} = 0 \qquad \psi_1 = 0 \text{ at } y^* = 0; \quad \psi_1 = 0 \text{ at } y^* = f(x^*)\ O(\delta^1)$$

$$\frac{\partial^2 \psi_2}{\partial y^{*2}} = -\frac{\partial^2 \psi_0}{\partial x^{*2}} \qquad \psi_2 = 0 \text{ at } y^* = 0;$$

$$\psi_2 = 0 \text{ at } y^* = f(x^*)\ O(\delta^2) \tag{11}$$

This leads to the following series solution for ψ in a straight

(15) Leal, L. G. *Laminar Flow and Convective Transport Processes*; Butterworth-Heinemann: Stoneham, MA, 1992.
(16) Van Dyke, M. *Perturbation Methods in Fluid Mechanics*; Academic Press: New York, 1964.

channel geometry with a wavy boundary.

$$\psi = y^*f + \delta^2\left(\frac{y^*f''}{6f^2} - \frac{y^{*3}f''}{6}\right) + O(\delta^4) \qquad (12)$$

The quantity f'' in the above expression denotes the second derivative of the function f with respect to the variable x^*. Recognizing that the solute velocity in the channel is related to the stream function by

$$U_s = \sqrt{U_x^2 + U_y^2} = \frac{\mu\Delta\phi}{\lambda}\sqrt{\left(\frac{\partial\psi}{\partial y^*}\right)^2 + \delta^2\left(\frac{\partial\psi}{\partial x^*}\right)^2} \qquad (13)$$

the streamline velocity is given by

$$U_s = \frac{\mu\Delta\phi}{\lambda}\sqrt{\left[f + \frac{\delta^2 f''}{6f^2}(1 - 3\psi^2)\right]^2 + \delta^2\psi^2\frac{f'^2}{f^2}} + O(\delta^4) \qquad (14)$$

where f' denotes the first derivative of f. The velocity field derived above may be further substituted in eq 5 to estimate the transit time required to travel over a period of the wavy wall as

$$\begin{aligned} t_w &= \lambda\int_0^1\left[\frac{1}{U_s}\sqrt{1 + \delta^2\left(\frac{\partial y^*}{\partial x^*}\right)_\psi^2}\right]\mathrm{d}x^* \\ &= \lambda\int_0^1\left[\frac{1}{U_s}\sqrt{1 + \delta^2\psi^2\frac{f'^2}{f^4} + O(\delta^4)}\right]\mathrm{d}x^* \\ &= \frac{\lambda^2}{\mu\Delta\phi}\int_0^1\left[\frac{1}{f} - \frac{\delta^2 f''}{6f^4}(1 - 3\psi^2)\right]\mathrm{d}x^* + O(\delta^4) \end{aligned} \qquad (15)$$

Upon integration, the above expression simplifies to

$$t_w = \frac{\lambda^2}{\mu\Delta\phi}(1 + \epsilon)\left(1 - \frac{4\pi^2\delta^2\epsilon^2}{3} + 4\pi^2\delta^2\epsilon^2\psi^2\right) + O(\delta^4) \qquad (16)$$

Note that the integration path chosen to derive the above expression lay along the solute streamlines in the channel geometry. These paths given by the contours of the stream function in the channel appropriately describe the trajectory of the solute molecules in the absence of molecular diffusion.

Thus, we see that an introduction of a wavy boundary in a straight channel geometry produces a variability in the transit time across different solute streamlines given by $4\pi^2\delta^2\epsilon^2\psi^2$ to the leading order. As discussed previously, this variability in transit time arises from a modification in the solute path length, the average streamline velocity, and spatial fluctuations in the streamline velocity. To leading order, the effect of the wavy boundary on each of these quantities is given by

path length:

$$L = \lambda(1 + \pi^2\delta^2\epsilon^2\psi^2)$$

average solute velocity:

$$\bar{U}_s = \frac{\mu\Delta\phi}{\lambda(1 + \epsilon)}\left(1 + \frac{\epsilon^2}{2} + \frac{2\pi^2\delta^2\epsilon^2}{3} - \pi^2\delta^2\epsilon^2\psi^2\right)$$

variability in solute velocity:

$$\left\langle\left(\frac{\bar{U}_s}{U_s} - 1\right)\right\rangle = \frac{\epsilon^2}{2} - \frac{2\pi^2\delta^2\epsilon^2}{3} + 2\pi^2\delta^2\epsilon^2\psi^2 \qquad (17)$$

As may be seen, the above analysis suggests that a sinusoidal variation in the channel width increases the path length along any streamline that grows quadratically in ψ as we approach the wavy wall. To the leading order, this effect contributes a factor of $\pi^2\delta^2\epsilon^2\psi^2$ to the overall variability in the transit time. Since the total potential drop along any streamline is constant, the increase in path length also leads to a decrease in the average streamline velocity, further contributing a factor of $\pi^2\delta^2\epsilon^2\psi^2$. The third and the remaining contribution of $2\pi^2\delta^2\epsilon^2\psi^2$ comes about from the variability in the solute velocity along the streamline as discussed earlier. Finally, the product of the average velocity $\bar{U}_s$ along a streamline given by eq 17 and the streamline path length L is not exactly $\mu\Delta\phi$ as might be expected from eq 6. This is because our formulation is normalized by the total flow in the narrow section, and the potential drop is reduced by the increase in the channel width due to the wavy wall. We may shift from constant current to constant potential drop by simply rescaling $\Delta\phi$.

Although the above results were derived for a straight channel geometry, the analysis may be readily extended to a curved channel profile with a large turn radius. As discussed earlier, in the limit when the wavelength of the periods along the inner wall is much smaller compared to the turn radius, i.e., $\lambda \ll R$, the effects of the wavy boundary and the channel curvature on the transit time are simply additive. In this situation, recalling that $\psi = 0$ and $\psi = 1$ at the outer and the inner walls of the channel, respectively, eqs 3 and 16 may be combined to yield the following leading order dependence, i.e., ignoring higher order terms of $O(\alpha^2, \delta^4, \alpha\delta^2)$, of the transit time on the channel parameters.

$$t(\psi) = t_0(1 - 2\alpha\psi + 2\alpha\beta\psi^2); \quad \beta = \frac{4\pi^2\delta^2\epsilon^2}{2\alpha} \qquad (18)$$

Here $t_0 = \theta_0^2R^2(1 + \epsilon)(1 - 4\pi^2\delta^2\epsilon^2/3)/(\mu\Delta\phi)$ denotes the leading order term describing the transit time to travel along the outer track of the channel over a period of wavelength $\lambda = \theta_0R$. Note that the above expression predicts an equal transit time along the inner and outer channel walls for a value of $\beta = 1$. As may be clearly seen from eq 18, to leading order, the quadratic variation in transit time with ψ introduced by the wavy inner wall cannot completely eliminate the solute dispersion produced by curved geometries, which is linear in ψ. However, the wavy boundary allows retardation of the solute molecules near the inner wall, thus reducing solute dispersion by minimizing variations in transit time across different solute streamlines.

In the absence of molecular diffusion, the path followed by the solute molecules is determined by the streamlines in a channel

geometry. In this situation, the variance introduced by the modified spiral geometry may be simply determined from the variation in the transit time across solute streamlines as

$$\sigma^2 = \left(\frac{\lambda}{t_0}\right)^2 \frac{\int_0^1 (t(\psi) - \bar{t})^2 C_0(\psi)\, d\psi}{\int_1^0 C_0(\psi)\, d\psi}; \quad \bar{t} = \frac{\int_0^1 t(\psi) C_0(\psi)\, d\psi}{\int_0^1 C_0(\psi)\, d\psi} \tag{19}$$

Here $C_0(\psi)$ represents the concentration distribution of the solute molecules across different streamlines at the entrance of the separation channel. While this distribution depends on the inlet conditions, the simplest approach is to assume solute molecules are distributed uniformly across the streamlines at the channel entrance; i.e., $C_0(\psi) = 1$. In this case, eq 19 predicts the following dependence of the slug variance upon exit from the separation channel given by

$$\left(\frac{\sigma}{W}\right)^2 = \left(\frac{\alpha}{\delta}\right)^2 \left(\frac{1}{3} - \frac{2}{3}\beta + \frac{16}{45}\beta^2\right) \tag{20}$$

It may be readily shown that the above expression is minimized for a value of $\beta = 15/16$ yielding an optimum choice for ϵ given by

$$\epsilon_{opt} = \frac{1}{\pi\delta}\sqrt{\frac{15\alpha}{32}} \tag{21}$$

Note that, for such a choice of channel parameters, the transit times along the inner and the outer channel walls are nearly equal[7] and the maximum differential in transit times is reduced by a factor of 4 over the simple spirals.

The effect of width profiling as predicted by the analytical model was verified by obtaining the solute concentration profile in these modified geometries numerically. In this calculation, the electric potential (ϕ) inside the channel was first determined by solving the governing Laplace equation $\nabla^2\phi = 0$ subject to the boundary conditions

$$\vec{\nabla}\phi.\, \vec{n}|_{y^*=0,1/f(x^*)} = 0;\ \phi|_{x^*=0} = 0;\ \phi|_{x^*=1} = 1 \tag{22}$$

The electrokinetic velocity, proportional to the local electric field strength, was then derived from this solution by evaluating $\vec{\nabla}\phi$ inside the channel. The above numerical analysis was carried out using the Partial Differential Equation Toolbox in MATLAB for different channel geometries. In the absence of molecular diffusion, the variation in the transit time across solute streamlines was captured using eq 5 as the solute molecules follow a deterministic trajectory given by the streamlines in the geometry. Results obtained from such an analysis have been depicted in Figure 4. As may be seen, the solute profile matches the quadratic profile predicted by the asymptotic model. Further, note that, for the case depicted in the figure, the optimum value of ϵ as predicted by eq 21 is 0.1, which occurs for nearly equal transit times[7] along the inner and the outer channel walls.

TAYLOR−ARIS DISPERSIVITY LIMIT

The above analysis neglects the effect of diffusion on the solute concentration profile in the channel and thus is appropriate for infinite Peclet number systems. However, the separation time in the spiral geometries is often much greater than the time required for the solute molecules to diffuse across the channel width; i.e., $LD/(\mu EW^2) \gg 1$. In this situation, it is more appropriate to describe analyte dispersion in terms of the Taylor−Aris dispersivity limit. As discussed earlier, such dispersion arises in the modified spiral geometries due to a variation in both the path length and the solute velocity across different streamlines. However, the two effects may be combined to obtain a modified velocity profile in the $x^* - \psi$ domain using a regular perturbation technique as presented in the previous section. It is important to note that from a Lagrangian perspective (e.g., in a frame of reference moving with a solute molecule) this flow field has both steady and periodic components that contribute[18−23] to the overall dispersion of the solute slugs in the separation geometry. While the steady component may be evaluated from the flow field averaged over a period of the wavy inner wall, the periodic component arises due to a variation in the channel width with axial distance as the solute slug moves through the geometry. Because the Peclet number is large for our systems, however, this latter contribution may be evaluated as the time-average dispersion due to oscillatory flow on each streamline. For an arbitrary unidirectional flow through a conduit of constant cross section, Watson[19] showed that the contributions of oscillatory and steady shear to overall dispersion are additive and that each could be computed separately. We shall assume the same to hold true in the modified geometries considered here.

To begin with, we focus on dispersion arising due to the oscillatory flow modes in a straight channel geometry with a wavy boundary. The asymptotic theory presented earlier shows that

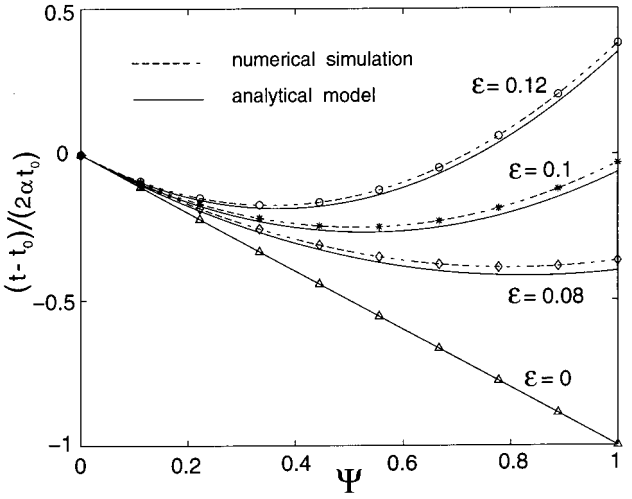

Figure 4. Variation in the transit time with stream function to travel over one period of the modified spiral geometry in the absence of molecular diffusion. For the above simulations, the normalized radius ($1/\alpha$) and the wave frequency (δ) were chosen to be 200 and 0.1541, respectively. The points in the figure refer to the values of ϵ at which numerical simulations were carried out.

(17) Aris, R. *Proc. R. Soc. London* **1956**, *235A*, 67−77.
(18) Aris, R. *Proc. R. Soc. London* **1960**, *259*, 370−376.
(19) Watson, E. J. *J. Fluid Mech.* **1983**, *133*, 233−244.
(20) Indeikina, A.; Chang, H. C. *Phys. Fluids A* **1993**, *5* (10), 2563−2566
(21) Goddard, J. D. *Phys. Fluids A* **1993**, *5* (9), 2295−2297.
(22) Krishnan, G. P.; Leighton, D. T. *Phys. Fluids A* **1992**, *4* (11), 2327−2331.
(23) Leighton, D. T. *PhysicoChem. Hydrodyn.* **1989**, *11*, 377−386.

the modified velocity profile in this geometry is given by $U_s(\partial x/\partial s)_\psi$, which upon simplification yields

$$v_s = \frac{\lambda}{t_0}\left(f + \frac{\delta^2 f''}{6f^2}(1 - 3\psi^2)\right) + O(\delta^4); \qquad f = \frac{1}{1 + \epsilon[1 - \cos(2\pi x^*)]} \quad (23)$$

Here again f'' is the second derivative of the function f with respect to x^*, δ is the dimensionless wave frequency, and ϵ is the dimensionless amplitude of the waves along the inner channel wall. As may be seen from eq 23, the modified velocity field in the wavy channel may be decomposed into oscillatory extensional and shear flow modes along with a spatially averaged steady shear flow component. To leading order, the oscillatory term in the modified flow profile arises from a periodic extensional flow component given by Uf, where $U = \lambda/t_0$. Solute dispersion introduced by such periodic extensional flows has been investigated by Krishnan and Leighton.[22] Their work demonstrates that the Taylor−Aris dispersivity in such systems is given by $\cosh(2\dot{\gamma}_e/\omega)I_0(2\dot{\gamma}_e/\omega)$, where $\dot{\gamma}_e$ and ω are the periodic strain rate and the angular frequency in the flow field, respectively. The symbol I_0 here denotes the zeroth order modified bessel function of the first kind. For small values of the dimensionless strain rate, i.e., $\dot{\gamma}_e/\omega \ll 1$, the above expression may be simplified to yield $1 + 3(\dot{\gamma}_e/\omega)^2$. Proceeding further, it may be readily shown that the strain rate arising due to the leading periodic extensional flow component scales with $Uf'/\lambda \sim 2\pi\epsilon U/\lambda$. Also recognizing that the frequency of the oscillations in the flow field is given by $2\pi U/\lambda$, the dimensionless strain rate, $\dot{\gamma}_e/\omega$, may be shown to scale with ϵ. Thus, the contribution to the overall solute dispersion from the periodic extensional flow component is an $O(3\epsilon^2)$ quantity. For the modified spiral geometries considered here, this contribution is negligible since $\epsilon \ll 1$.

In addition to dispersion arising due to the oscillatory extensional flow mode, the periodic shear flow also contributes to the overall spread in the solute slugs. Work dating back to the seminal paper of Aris[18] has shown that the dispersivity is proportional to the square of the amplitude of the periodic strain and that it approaches a finite maximum for frequencies ω such that $\omega W^2/D \gg 1$. This high-frequency limit corresponds to periods that are much shorter than the time necessary for solute to diffuse across the channel. As the characteristic time period for the oscillatory flow components in the channel is given by λ/U, this high-frequency limit corresponds to the situation when $(W^2U)/(\lambda D) = \delta Pe \gg 1$, which is again satisfied for the cases considered here.

In the high-frequency limit, Leighton[23] showed that the total dispersion in a channel could be calculated from the Taylor−Aris dispersion along each streamline. This dispersivity due to the oscillatory shear flow component in the modified spiral geometry has an upper bound given by

$$\left(\frac{\hat{K}}{D}\right)_s \sim \frac{1}{2}\left(\frac{\dot{\gamma}_s}{\omega}\right)^2 \sim 2\pi^2\epsilon^2\delta^2\psi^2 \quad (24)$$

Therefore, the upper bound to the overall dispersivity due to the periodic shear flow component may be obtained as

$$\left(\frac{K}{D}\right)_s = \int_0^1 \left(\frac{\hat{K}}{D}\right)_s d\psi \sim \frac{2}{3}\pi^2\epsilon^2\delta^2 \quad (25)$$

Thus, we see that the contribution arising from the periodic shear flow component may be neglected as well since ϵ and δ are typically $O(0.1)$ quantities for geometries considered here. However, it is important to note that while the contributions from the oscillatory flow modes are negligible for gentle spiral geometries, they become significant for compact spiral profiles when $\alpha \rightarrow O(1)$. For such geometries, the asymptotic analysis presented above is inapplicable since the value of ϵ and δ required to reduce dispersion arising from the channel curvature also become $O(1)$ quantities.

Although the above analysis was carried out for a straight channel geometry with a wavy boundary, it may be readily extended to a curved channel profile. In this case, additional oscillatory flow modes of $O(\alpha)$ also contribute to the overall solute dispersion in the separation geometry. Again, as $\alpha \ll 1$ for the spiral profiles considered here, these contributions are insignificant in determining the performance of the modified spiral geometries.

The key difference between the contribution of oscillatory and steady flow modes to dispersion is that oscillatory modes are always of $O(\epsilon^2,\epsilon^2\delta^2$, etc.) at large Pe, while the steady modes are of order $(\alpha Pe)^2$. Thus, at large Pe, such as considered here, the contribution from steady modes will always be dominant. This contribution results from the spatially averaged velocity field given by

$$v_s(\psi) = v_0(1 + 2\alpha\psi - 4\pi^2\delta^2\epsilon^2\psi^2) \quad (26)$$

where $v_0 = \lambda/t_0$ is the average solute velocity along the outer track of the spiral channel. Note that the flow field given above takes into account the modifications in the streamline velocity as well as that in the path length along a streamline due to channel curvature and wavy inner wall. For such a velocity profile, the Taylor−Aris dispersivity in the channel may be readily obtained using the method of moments[17] to yield

$$\frac{K}{D} = 1 + [\alpha(1 + \epsilon)Pe]^2\left(\frac{1}{30} - \frac{\beta}{15} + \frac{32\beta^2}{945}\right); \quad \beta = \frac{4\pi^2\delta^2\epsilon^2}{2\alpha} \quad (27)$$

where $Pe = (v_0W)/D$. The above expression suggests that solute dispersion in the modified spirals exhibits a minimum value for $\beta = 63/64$. Note that this value is close to both 15/16 and unity, suggesting that the equal transit time[7] condition along the inner and outer channel walls is nearly optimum at both infinite Pe and Taylor−Aris dispersion limits. Further, for such optimum profiles, the Taylor−Aris dispersivity arising from the shear flow in the system is reduced by a factor of 64 over the unmodified spirals.

To verify the predictions of the analytical model, Monte Carlo simulations were performed to estimate the Taylor−Aris dispersivity in the modified spiral geometries. These simulations were based on a deterministic velocity profile obtained numerically by solving the convective flow equations and coupled with a random

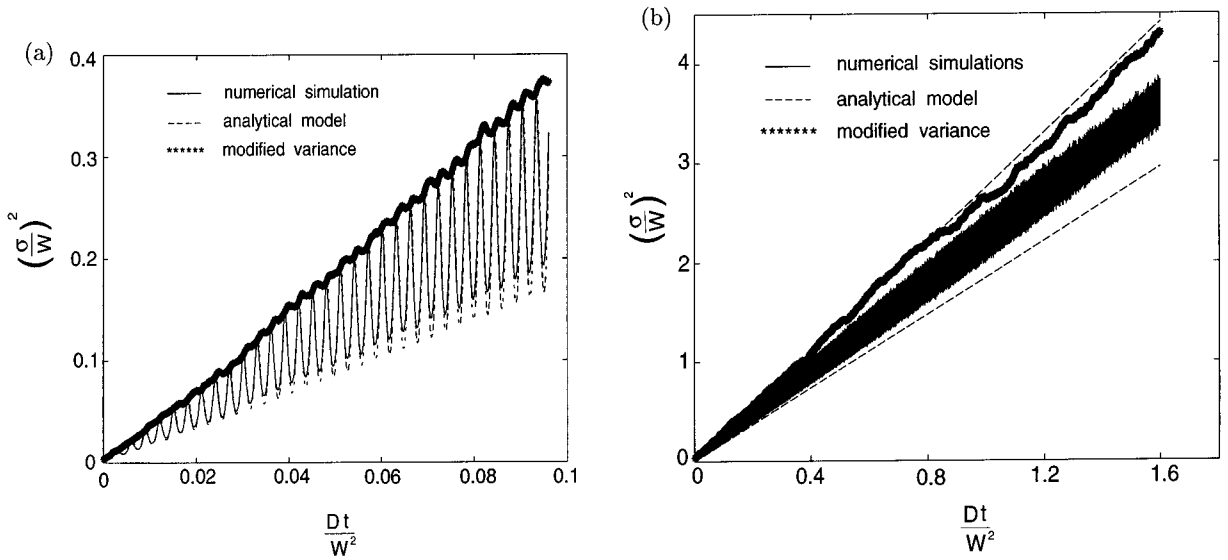

Figure 5. Growth of slug variance in the modified spiral geometries involving contributions from both hydrodynamic dispersion and molecular diffusion. For this case, the channel parameters chosen were (a) normalized radius $1/\alpha = 200$, normalized wave frequency $\delta = 0.0796$, normalized amplitude for the waves $\epsilon = 0.2$, and Peclet number $Pe = 5000$; and (b) $1/\alpha = 200$, $\delta = 0.1591$, $\epsilon = 0.1$, and $Pe = 3000$. The dotted lines in (b) represents the upper and lower envelopes for the slug variance as predicted by eq 28.

walk diffusion model.[24] Molecules at each time step of size Δt were randomly displaced in the x and y directions by an amount governed by a Gaussian distribution with standard deviation $\xi = (2D\Delta t)^{1/2}$, where D is the molecular diffusivity of the system. Further, the molecules were appropriately reflected off the channel walls to capture the effect of free slip boundary conditions on the Taylor−Aris dispersivity. In Figure 5 we have depicted the variation in the slug variance with time as predicted by the Monte Carlo simulations. As may be seen, the solute slug gets stretched and compressed due to a periodic variation in the channel width with axial distance as it travels around the separation column. It is important to note that, for the modified spiral geometries chosen here, the convective time scale to travel over a period of the spiral is often much smaller compared to the time scale for transverse diffusion to set in $\lambda/v_0 \ll W^2/D$ or $\delta Pe \gg 1$. In this situation, we may ignore the effect of molecular diffusion over a period of the oscillating slug variance. Moreover, the oscillations in the slug variance may be taken into account in the analytical model by describing these fluctuations from a frame of reference moving with the average velocity of the analyte band. Thus, to leading order, the amplitude and the frequency of the oscillating slug variance would be identical to that of the square of the mean velocity field as experienced by the traveling solute band. In this situation, the slug variance may be described as

$$\left(\frac{\sigma}{W}\right)^2 = \frac{1}{W^2}\frac{2Kt}{[1-\epsilon(1-\cos(2\pi\bar{v}t/\lambda))]^2}; \quad \bar{v} = \int_0^1 v_s(\psi)\,d\psi \tag{28}$$

Here K is the Taylor−Aris dispersivity estimated using eq 27 and $v(\psi)$ is the velocity profile as given by eq 26. The growth in the slug variance with time as predicted by eq 28 has been presented in Figure 5. As may be seen, the analytical model describes solute dispersion in the spiral geometries quite well. Note that eq 28 predicts a linear growth in the amplitude of the oscillation in the slug variance with time. However, the Monte Carlo simulations show that such a linear growth occurs only at short times, i.e., $t \ll O(\lambda^2/(2K))$, when the slug variance is small as compared to λ^2, where λ is the wavelength of the periods in the modified spirals. At larger times, the deviation between the analytical and the Monte Carlo results becomes significant. This occurs because the solute slug is spread over several periods of the wavy channel, and thus, different regions of the slug no longer undergo compression or elongation simultaneously as assumed in the analytical model. Under these conditions, the amplitude of the oscillation in the slug variance asymptotes to a constant, as may be seen in Figure 5b.

To compare the performance of the various spiral separation geometries, it is important to choose a useful way of estimating the Taylor−Aris dispersivity in the modified spiral geometries which is fluctuating with time. Because in our analysis we compare different geometries for a given minimum channel width, this may be appropriately achieved by mapping the analyte concentration profile in the modified geometries to that which would occur if the slug was suddenly withdrawn into an uniform spiral channel of width W. Mathematically, this corresponds to a modification in the angular distance between every (i, j) molecule pair to

$$\Delta\theta_{ij}^* = \frac{1}{W}\int_{\theta_i}^{\theta_j} w(\theta)\,d\theta; \quad w(\theta) = W\left[1+\epsilon-\epsilon\cos\left(\frac{2\pi\theta}{\theta_0}\right)\right] \tag{29}$$

where θ_i and θ_j are the angular positions of the ith and the jth molecule in the modified spiral geometry at any instant. Such a mapping not only allows appropriate comparison of the various channel geometries but also diminishes the oscillatory variation in the slug variance as it travels around the spiral (see Figure 5). We thus compare the simple spiral and the various modified spiral geometries in terms of the growth rate of this modified variance.

(24) Fogelson, A. L. *J. Comput. Phys.* **1992**, *100*, 1−16.

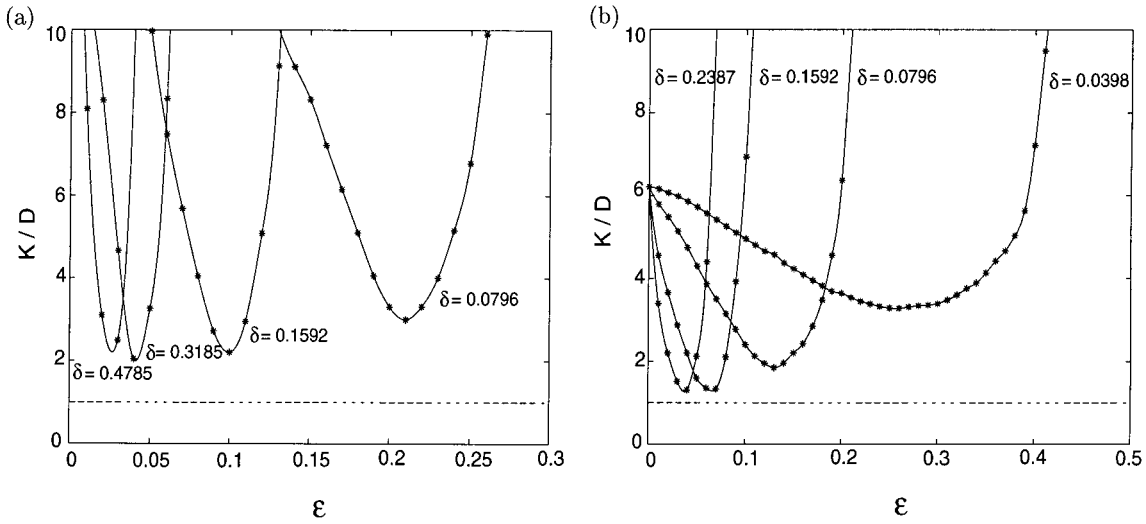

Figure 6. Dependence of the solute dispersivity on the amplitude of width variation for the modified spirals at $Pe = 5000$: (a) $\alpha = 1/200$; (b) $\alpha = 1/400$. The dotted line represents a value of $K/D = 1$, the minimum achievable value.

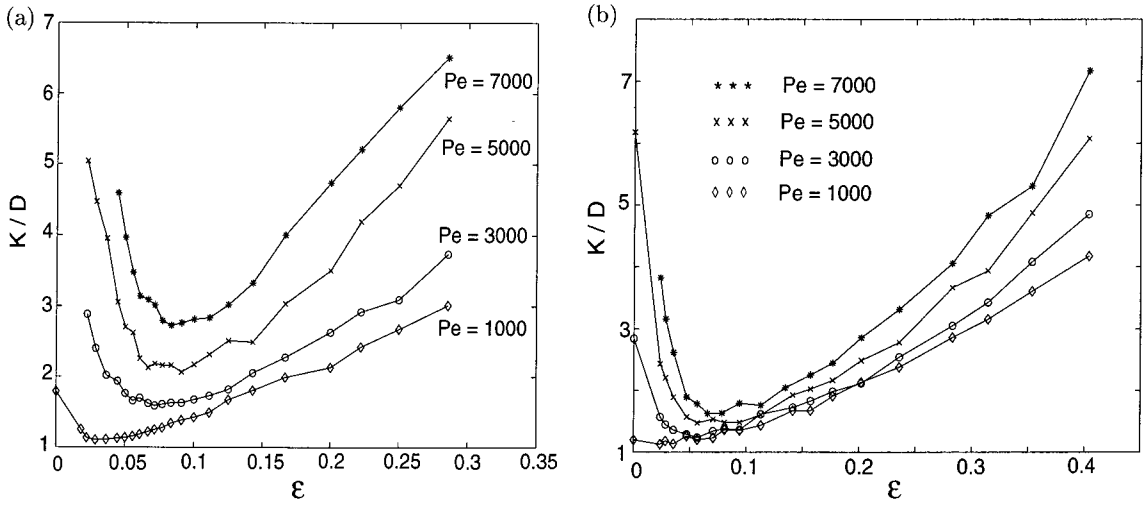

Figure 7. Effect of the amplitude of width variation on analyte dispersion in modified spiral geometries satisfying $\beta = 1$: (a) $\alpha = 1/200$; (b) $\alpha = 1/400$.

To begin with, the dependence of the solute dispersivity on the amplitude of the periods of a given wavelength was explored. As depicted in Figure 6, simulation results indicate a strong dependence of the Taylor−Aris dispersivity on this parameter, as may be expected from the large *Pe* results. Moreover, the modified Taylor−Aris dispersivity exhibits a sharp minimum for values of ϵ close to that predicted by the analytical model, i.e., $\beta = 63/64 \Rightarrow \epsilon_{opt} = (63\alpha/128)^{1/2}/(\pi\delta)$, which occurs for nearly equal transit times along the inner and outer channel walls. On the basis of this observation, the modified spiral designs were further investigated by assuming an optimum behavior for profiles satisfying this equal transit time criterion based on the asymptotic theory; i.e., $\beta = 1$. The performance of such geometries has been depicted in Figure 7 as a function of ϵ. As may be seen, for larger values of ϵ, the analyte dispersion in the modified geometries grows due to an increase in the average width of the channel. Moreover, the numerical simulations predict an optimum amplitude for the waves along the inner wall not captured by the analytical model. This occurs because the correction introduced by the wavy inner wall diminishes in the limit $\epsilon \rightarrow 0$ and the performance of the modified geometries approach that of the simple spiral of same normalized radius and channel width. In this limit, the asymptotic model fails as the optimum values of δ desired to minimize solute dispersion in the modified spiral geometries are $O(1)$ or higher.

The optimization carried out above readily yields an estimate for the enhancement in the separation performance achievable using the proposed width profiling strategy over the unmodified spirals. To see this, we have compared the performance of the optimally modified spirals to that of the simple spirals in Figure 1. As may be seen, for a given normalized radius, the modified spiral geometry diminishes the Taylor−Aris dispersivity arising due to the channel curvature by as much as a factor of 64 as predicted by the asymptotic theory. This in turn suggests that the operating Peclet number for the spiral designs may be increased by as much as a factor of 8 without compromising the performance, rendering the spiral separation geometry effective even for large *Pe* systems such as employed in matrix based separations. In Figure 8a, we have compared the performance of the modified spiral geometries with the simple spirals for different values of the normalized radius. As may be seen, for $\alpha Pe < O(\sqrt{30})$, there is little improvement achieved by adding a wavy

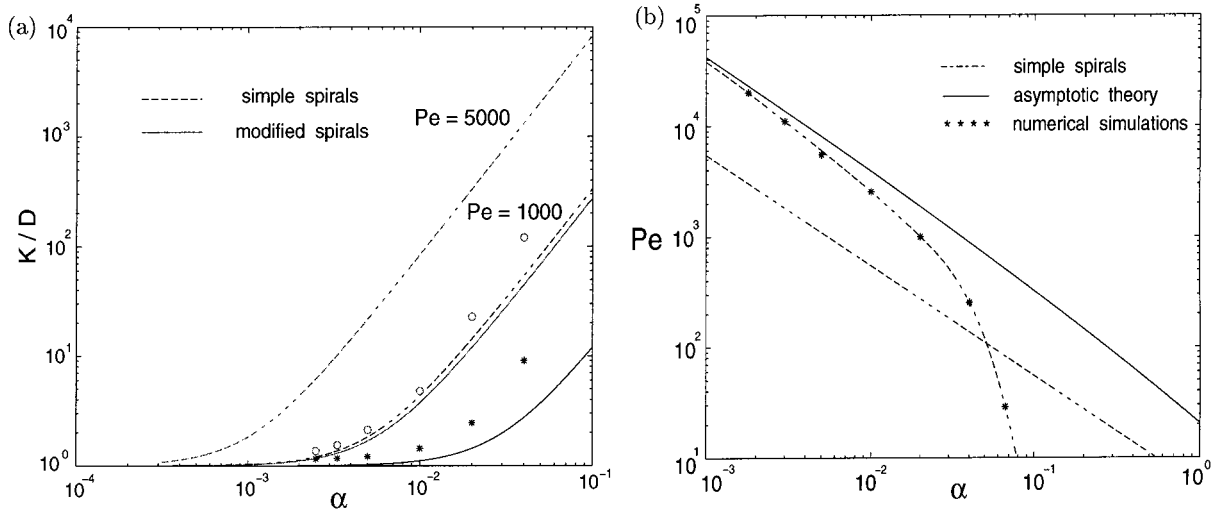

Figure 8. (a) Effect of the aspect ratio on the performance of the wavy profiles and the simple spirals: (*) $Pe = 1000$; (○) $Pe = 5000$. (b) Parameter space for which geometric dispersion in the spiral profiles equals that due to ordinary axial diffusion. In both (a) and (b), for the modified spiral geometries δ was chosen to be 0.2 and the value of ϵ was derived for $\beta = 1$. Dashed lines are unmodified spiral results (eq 4) while solid lines represent the analytical model for wavy channels.

inner wall because in this case dispersion is dominated by ordinary axial diffusion. For larger αPe, however, the improvement is substantial, exceeding 1 order of magnitude for $\alpha = 0.01$ and $Pe = 5000$. A close agreement between the simulation results and the asymptotic theory for $\alpha < O(0.01)$ and $\alpha Pe \gg O(\sqrt{30})$ shows that such width profiling allows the shrinkage of the spiral designs by as much as a factor of 8 in this limit to achieve the same dispersion, which may be important in microchip design. Note that, for a given Pe, the benefit again diminishes for larger values of α due to the large amplitude of the width profile required to equate transit times.

The above analysis clearly shows that simple spiral separation geometries are effective for systems with $\alpha Pe \leq O(\sqrt{30})$. Thus, in a parameter space of α and Pe, the contribution to solute dispersion from the channel curvature is less than that arising due to ordinary axial diffusion in the region beneath the dotted line in Figure 8b. The asymptotic theory predicts that this region may be extended to that beneath the solid line by adding a wavy inner wall of appropriate amplitude and wavelength. However, the contribution to slug dispersion from the higher order flow modes, ignored in the asymptotic model, restricts this region to that beneath the curve traced by the numerical simulation results (*). From the intersection of these curves, it is apparent that the wavy profile design is superior for $Pe \geq O(100)$. At $Pe = 5000$, typical for matrix-based DNA separations,[25] for example, designs yielding minimal dispersion may be 6 times more compact than a simple spiral, a significant step in miniaturization.

CONCLUSIONS

In summary, we have investigated a simple width profiling strategy that significantly reduces solute dispersion around curved channels on microchip geometries. It is known from previous studies[10] that, for any given curved profile and normalized turn radius, the dispersivity is minimized for the smallest channel width. If the channel width is fixed, dispersion may be minimized by employing gentle spiral geometries[1] (small $\alpha = W/R$). However, such a strategy is most effective only for systems with $\alpha Pe < O(\sqrt{30})$. For systems with $\alpha Pe > O(\sqrt{30})$, a substantial additional improvement is possible if a wavy wall of appropriate wavelength and amplitude is introduced along the inner track of the channel. Analysis suggests that such profiling increases the transit time along a streamline that grows quadratically in the stream function ψ to the leading order as we approach the wavy wall and thus cannot eliminate dispersion introduced by the channel curvature, which is linear in ψ. In this situation, analytical and numerical studies show that dispersion is minimized for nearly equal transit times along the inner and the outer tracks of the channel.[7] Moreover, the overall dispersion of solute slugs in these modified spiral geometries is dominated by the contribution from the steady shear flow component at large Pe provided $\epsilon, \delta \ll 1$, as is the case here. Numerical simulations show that a reduction in solute dispersion by as much as a factor of 64 may be obtained using the optimally modified profiles over the simple spirals. This permits the increase in the operating Pe by nearly a factor of 8 for the same solute dispersion. Alternatively, at a fixed Pe and minimum channel width, the profiling of the inner wall permits a shrinkage of the radius of the spiral separation geometry by an identical factor. The latter benefit may be of greater importance for optimal compact microchip separation channel design. Finally, the requirement that $\alpha \ll 1$ limits the applicability of the design to systems for which $Pe \gtrsim O(100)$, common to most matrix-based separations.

ACKNOWLEDGMENT

This research work was supported by the National Science Foundation Grant CTS-9980745.

Received for review June 27, 2001. Accepted November 26, 2001.

AC010718C

(25) Bousse, L.; Cohen, C.; Nikiforov, T.; Chow, A.; Kopf-Sill, A. R.; Dubrow, R.; Parce, J. W. *Annu. Rev. Biophys. Biomol. Struct.* **2000**, *29*, 155−181.